



# Microbial Inactivation by Non-equilibrium Short-Pulsed Atmospheric Pressure Dielectric Barrier Discharge (Cold Plasma): Numerical and Experimental Studies

Ender H. Arserim<sup>1</sup> · Deepti Salvi<sup>1</sup> · Gregory Fridman<sup>2</sup> · Donald W. Schaffner<sup>1</sup> · Mukund V. Karwe<sup>1</sup>

Received: 14 January 2020 / Accepted: 14 September 2020 / Published online: 20 October 2020  
© Springer Science+Business Media, LLC, part of Springer Nature 2020

## Abstract

Microbial inactivation efficacy of plasma generated by a custom-made floating electrode dielectric barrier discharge (FE-DBD) or cold plasma at three different frequencies (1 kHz, 2 kHz, and 3.5 kHz) was experimentally evaluated for its inactivation of the pathogen surrogate *Enterobacter aerogenes* on a glass surface to obtain inactivation kinetics. COMSOL Multiphysics® was used to numerically simulate the amount and the distribution of reactive species within an FE-DBD system. Microbial inactivation kinetics was predicted using species concentrations and microbial inactivation rates from the literature and compared with experimental data. The results showed that the FE-DBD plasma treatment achieved a microbial reduction of  $4.3 \pm 0.5$  log CFU/surface at 3.5 kHz,  $5.1 \pm 0.09$  log CFU/surface at 2 kHz, and  $5.1 \pm 0.05$  log CFU/surface at 1 kHz in 2 min, 3 min, and 6 min, respectively. The predicted values were 4.02 log CFU/surface, 4.10 log CFU/surface, and 4.56 log CFU/surface at 1 kHz, 2 kHz, and 3.5 kHz, respectively. A maximum 1 log difference was observed between numerical predictions and the experimental results. The difference might be due to synergistic interactions between plasma species, UV component of FE-DBD plasma, and/or the electrical field effects, which could not be included in the numerical simulation.

**Keywords** Dielectric · Barrier discharge plasma · Microbial inactivation · Mathematical modeling · Inactivation kinetics

## Introduction

Significant effort and resources have been directed towards improving the efficiency and sustainability of the food supply chain. Besides developing new approaches for reducing food waste and reducing energy consumption, there is a growing demand for high-quality food products that are minimally processed, safe, and affordable. The development of novel nonthermal food preservation processes is of great interest for minimally processed foods. Researchers seek to increase food safety and enhance shelf life while maintaining important food quality attributes. One emerging nonthermal technology that may help is cold atmospheric pressure

plasma (CAPP). The antimicrobial efficacy at or near room temperature of cold plasma makes it desirable to process temperature-sensitive foods [49].

Plasma, the fourth state of matter, can be described as a partially or fully ionized gas [32]. If enough energy is applied to a gas, this breaks apart interactions between molecules and atoms, which results in the generation of charged and neutral species, including ions, electrons, and free radicals, while releasing radiation at different wavelengths. The mixture of species and radiation is called plasma. Plasma can be classified as a hot plasma or cold plasma, depending upon its temperature. The Sun and the interior of stars are examples of hot plasma, and the Aurora Borealis is an example of cold plasma in our universe [7]. This research is focused on non-equilibrium short-pulsed discharge, or “cold plasma” in which the temperatures of neutral and reactive species are at or near room temperature while electrons are at  $\sim 1$  eV ( $\sim 10^4$  K).

Different theories have been developed to explain the antimicrobial effects of CAPP. The most common proposed mechanism of action is the oxidation of cell constituents which is attributed to reactive oxygen such as

✉ Mukund V. Karwe  
mkarwe@sebs.rutgers.edu

<sup>1</sup> Department of Food Science, Rutgers, The State University of New Jersey, 65 Dudley Road, New Brunswick, New Jersey 08901, USA

<sup>2</sup> C. & J. Nyheim Plasma Institute, Drexel University, 200 Federal St. Suite 500, Camden, New Jersey 08103, USA

superoxide ( $O_2^-$ ), hydrogen peroxide ( $H_2O_2$ ), hydroxyl radicals (OH), ozone ( $O_3$ ), and reactive nitrogen species such as nitric oxide (NO) and others. The interactions between these reactive species and cellular macromolecules, such as lipids, proteins, and DNA, can result in the death of the cell [4, 11, 42].

Researchers have shown that CAPP can effectively inactivate different microorganisms with high food quality retention [2, 12, 13, 50]. Some research has suggested that plasma has adverse effects on some food quality parameters changing color and contributing to oxidation [23, 25, 34]. While some microorganisms (e.g., *Escherichia coli*) are more susceptible to plasma, spore-forming bacteria such as *Bacillus subtilis* are less so [20, 30, 33]. Different plasma generation methods can also affect the degree of microbial inactivation observed [5, 39, 45].

While the application of plasma technologies to inactivate microorganisms has been studied, the prediction of microbial inactivation kinetics would allow the comparison of different plasma process technologies on the reduction of microbial populations. Very few studies have focused on the mathematical modeling of microbial inactivation by cold plasma treatment. Some studies have focused on microbial inactivation by plasma as functions of time, process gas type, gas flow rate, frequency, or voltage [48, 49]. While many of the operating parameters for the plasma generating equipment can affect the amount and type of molecular species generated, microbial inactivation by cold plasma has been ascribed mainly to the reactive species [8, 15]. A generalized reactive species-based microbial inactivation model would allow comparison between studies and might point a way toward more effective treatment conditions.

The overarching goal of this study was to investigate the microbial inactivation efficacy of CAPP on *Enterobacter aerogenes* in a model system and develop a mathematical model to predict microbial inactivation kinetics. A key objective was to predict the plasma species distribution and concentration at a microbially contaminated surface, and couple it with the microbial inactivation kinetics from the literature to predict the microbial inactivation level and compare with experimental data. The transport of reactive species was numerically solved to obtain species distribution between plasma electrodes in a custom made floating electrode dielectric barrier discharge (FE-DBD) device (Drexel University, PA). The same equipment was used to conduct microbial inactivation experiments [10]. Numerical simulation of reactive species distribution was carried out by using COMSOL Multiphysics®. Numerically predicted reactive species concentrations and their distributions were coupled with microbial inactivation rate from the literature to estimate microbial inactivation, and the results were compared with experimental data.

## Material and methods

### Interacting surface

Since surface roughness can affect the microbial inactivation efficacy of cold plasma [3, 21]. Fisherbrand™ glass microscope slide (0.001 m × 0.0254 m × 0.0762 m) was used as a model surface. The surface roughness of these glass slides was  $0.28 \pm 0.02 \mu\text{m}$  [21], which is smaller than a typical microbe, and therefore, it could be considered a “smooth” surface. *Enterobacter aerogenes* (0.6–1.0  $\mu\text{m}$  in diameter and 1.2–3.0  $\mu\text{m}$  long) were spot inoculated on the glass slide surface in an area with dimensions of 0.0254 m × 0.0254 m. Microbial inactivation results were reported in terms of log CFU per area (1 in<sup>2</sup> or 0.000645 m<sup>2</sup>).

### Bacterial culture

Nalidixic acid-resistant *Enterobacter aerogenes* B 199A (Vivolac Cultures, Indianapolis, IN) is a non-pathogenic, gram-negative bacterium [31], with similar attachment characteristics to *Salmonella* spp. [53]. Prior research has shown that *Enterobacter*, *Salmonella*, and four other Enterobacteriaceae (*Escherichia*, *Citrobacter*, *Arizona*, and *Shigella*) are part of a single, large cluster within the Enterobacteriaceae, with little or no evidence of subdivisions into tribes or genera when analyzed according to 105 different features including biochemical and physiological characteristics [28]. Nalidixic acid inhibits the growth of other microorganisms and allows the growth of only *E. aerogenes* B 199A strain.

The frozen bacterial culture was stored at  $-80^\circ\text{C}$  in 80% sterile glycerol. Bacteria from frozen stock were transferred, and the quadrant was streaked onto Tryptic Soy Agar (BD Difco, Sparks, MD) containing 50  $\mu\text{g/ml}$  nalidixic acid (Sigma Chemical Co., St. Louis, MO) (TSA-na) and incubated at  $37^\circ\text{C}$  for 24 h. One colony of the bacterium was transferred to 30 ml of Bacto Tryptose Soy Broth (Bacto, BD, Sparks, MD) containing nalidixic acid (50  $\mu\text{g/ml}$ ) and incubated at  $37^\circ\text{C}$  for 24 h. The final bacterial concentration of suspension was  $8.27 \pm 0.11$  log CFU/ml. This suspension was used for all microbial inactivation experiments.

### Floating electrode dielectric barrier discharge Plasma (FE-DBD)

The FE-DBD (at Drexel University, Camden, PA) system used in our experiments is shown in Fig. 1. The system uses a microsecond-pulsed power supply in which sinusoidal discharges were generated between two electrodes, as shown in Fig. 1 a and c. The rounded powered copper electrode was

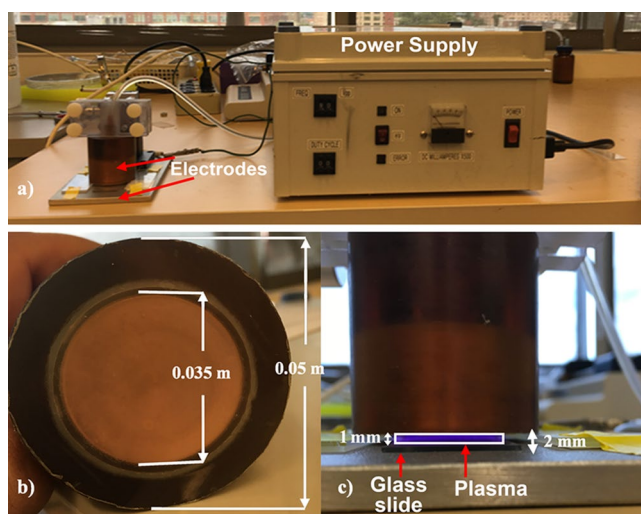


**Fig. 1** a FE-DBD or cold plasma unit (electrodes and power supply). b Powered copper electrode (0.035 m diameter) and clear fused quartz (0.05 m diameter and 0.001 m thick). c The purple glow is the plasma generated between the electrodes

0.035 m in diameter (Fig. 1b). Its open end was covered with 0.05 m diameter and a 1-mm-thick clear fused quartz (Technical Glass Products, Painesville, OH), and the copper electrode was enclosed in polyetherimide (Ultem) (Fig. 1b). The ground electrode was a standard stainless-steel plate (0.15 m × 0.25 m) placed at 2 mm from the quartz surface (Fig. 1c).

### Electrical Characterization of Plasma

The power supply was connected to a power analyzer, and the power required measured by a wattmeter (Electronic Educational Device, Denver, CO, USA). Power was measured five times when the plasma system was operated at each of three different frequencies (1 kHz, 2 kHz, and 3.5 kHz) with a 0.001 m air gap between a high-voltage electrode and a glass slide (1 mm thick). The distance between electrodes was increased (~ 50 mm) to measure power when the same voltage was applied, but no plasma was generated. The difference between the two measurements was reported as the power consumed in the generation of plasma. The average values of power of this FE-DBD system were  $4.80 \pm 0.5$  W,  $11.18 \pm 0.2$  W, and  $15.13 \pm 0.3$  W at 1 kHz, 2 kHz, and 3.5 kHz, respectively. The power of the plasma was divided into the number of pulses for each frequency to obtain power consumed per cycle or pulse. The average power of the FE-DBD plasma system per cycle was  $5 \times 10^{-3}$  W/cycle. Average power per cycle was used in the numerical simulation for the energy input of FE-DBD.

**Table 1** Experimental conditions for FE-DBD plasma

Frequency (kHz)	1	2	3.5
Exposure time (s)	0	0	0
	90	45	30
	180	90	60
	270	135	90
	360	180	120

### Experimental design for FE-DBD Plasma treatment

The bacterial suspension of *E. aerogenes* (50  $\mu$ l) was spot inoculated directly from the broth to the glass surface (area of 0.0254 m × 0.0254 m). The glass slide was held in a laminar flow biosafety cabinet for 2 h at room temperature for drying before treatment. The glass slide was exposed to plasma for different exposure times and at different plasma power cycles using the FE-DBD plasma system at conditions shown in Table 1.

After plasma treatment, the glass slide was transferred to a sterile bag with 20 ml 0.1% peptone broth (BD Difco, Sparks, MD), gently massaged to dislodge any viable cells on the slide. The 0.1% peptone containing any viable cells was serially diluted further in 0.1% peptone as needed (mostly 3 times, tenfold at a time) and 0.1 ml of peptone water was plated on tryptic soy (enriched with 50  $\mu$ g/ml nalidixic acid) agar on duplicate plates. Plates were incubated at 37 °C for 24 h. The number of colonies between 30 and 300 were reported. Each treatment condition was repeated 5 times.

The detection limit was calculated based on a single viable cell being recovered in 0.1 ml from the original 20 ml massaged with the glass slide ( $1 \text{ CFU}/0.2 \text{ ml} \times 20 \text{ ml} = 100 \text{ CFU}/\text{slide}$  or  $2 \log \text{ CFU}/\text{slide}$ ).

### Optical emission spectroscopy

An optical emission spectrometer (OES) by AvaSpec-ULS2048L-EVO (Avantes, Broomfield, CO, USA) was used to relatively quantify the presence of reactive (and potentially antibacterial) species in the CAPP. The OES had a 2-m-long 600- $\mu$ m fiber cable with an F400 COL-UV/VIS collimating lens in the range from 200 to 1100 nm. The Avasoft8 software recorded the relative absorbance value of species. Each measurement was performed three times with an integration time of 10,000 ms and was recorded as emission spectra. The spectral peaks were then identified

and processed by using the Avast8 software and spectrum analyzer for the presence of reactive species (v1.7, Brno, Czech Republic).

## Statistical analyses

Statistical analyses were performed using SPSS software (version 24.0 IBM Corp, NY). All experimental data were subjected to one-way analysis of variance (ANOVA), and means were compared using the Tukey method with a 95% confidence interval.

## Mathematical modeling

The mathematical model numerically solved for the diffusion of generated reactive species and their secondary reactions to predict the concentrations and distributions of the reactive species in the FE-DBD plasma zone and on the glass surface. COMSOL Multiphysics® (version 5.4) transport of diluted species sub-module under the chemical engineering module was used to predict distributions and concentrations of reactive species. The calculated surface concentration of reactive species was used to predict microbial inactivation kinetics of *E. aerogenes*, and the details are described in the following sections.

## Geometry

The model addressed the cylindrical domain between the two electrodes with a glass slide on the bottom surface. The problem was assumed to be 2D axisymmetric without swirl to reduce computational time, so the computational domain consisted of a radial slice (center to edge) between the two electrodes. When revolved around the vertical (*y*) axis, this covers the entire domain under consideration. The radial slice implies that the glass slide area was circular, so the square inoculated region on the glass slide in the simulation was approximated as a circle. The domain included the region between the high-voltage electrode, which had a radius of 0.0175 m and the ground electrode. There was a 0.002-m gap between the electrodes, and the glass slide was 0.001 m thick, but it did not cover the entire region between the electrodes (see Fig. 2).

## FE-DBD Plasma chemistry

Plasma has complex chemistry due to the numerous potential reactions and generation of the many possible species, especially when the air is used as the gas supply. The FE-DBD

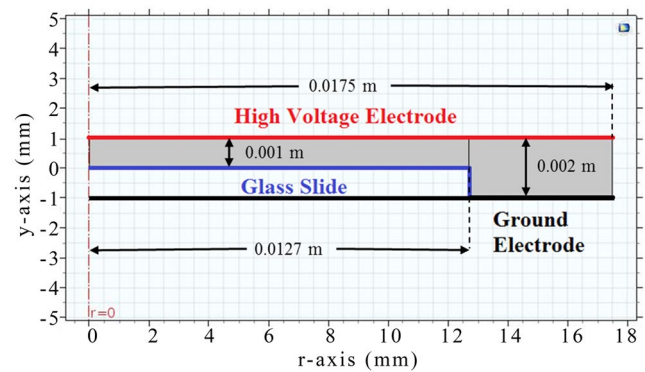


**Fig. 2** Radial cross section of computational domain showing the region between the electrodes and the glass slide. The computational domain is shown in gray for FE-DBD (the radius of high voltage electrode was 0.0175 m, the gap between electrode and glass slide was 0.001 m, and the length of glass slide was 0.0254 m)

system generated a thermodynamically non-equilibrium cold plasma [7], where the plasma temperature was near or at room temperature. The primary reactive species generated in the FE-DBD air plasma that has high antimicrobial inactivation activity are  $O^{\bullet}$ , OH,  $O_3$ , and  $H_2O_2$  [15]; [49], so only these species were included in the mathematical model describing the transport of the species.

The rate of reactive species generation in cold plasma can be obtained by using the species G-value from the literature, which represents the number of active species molecules generated by specific input energy (molecules per 100 eV). It can be expressed as a function of the SIE (specific input power) and the removed/produced amount of gas ( $\Delta C$ ), in a general form [24].

$$G - value(molecules \text{ per } 100eV) = \frac{\Delta C}{SIE} \times 1.6 \times 10^{-19} \quad (1)$$

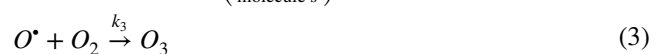
where  $\Delta C$  is the number of plasma species produced (molecules/ $m^3/s$ ), and *SIE* is the specific input power (W/ $m^3$ ).

The G-value of  $O^{\bullet}$  and OH, and reactions (2) and (3), were used to obtain the generation of the  $O^{\bullet}$ , OH,  $O_3$ , and  $H_2O_2$  species for the FE-DBD plasma system. Reactions (2), (3), (4) and (5) were used for the decay of  $O^{\bullet}$ , OH,  $O_3$ , and  $H_2O_2$ , species in the model, respectively.



$$G_{OH} = 9 \left( \frac{\text{molecule}}{100eV} \right) [9]$$

$$k_2 = 2.81 \times 10^{-18} \left( \frac{m^3}{\text{molecule} \cdot s} \right) [35]$$



$$G_{O^{\bullet}} = 3.2 \left( \frac{\text{molecule}}{100\text{eV}} \right) [9]$$

$$k_3 = 3.01 \times 10^{-17} \text{m}^3 / (\text{molecule} \cdot \text{s}) [35]$$



$$k_4 = 8.58 \times 10^{-2} \frac{1}{\text{s}} [35]$$



$$k_5 = 5.22 \times 10^{-6} \frac{1}{\text{s}} [35]$$

## Governing equations for predicting the distribution of charged species

It was assumed that the air/plasma column between two electrodes was stagnant, and mass diffusion was the only mass transfer mechanism. The governing mass transfer equation of diffusion of species is

$$\frac{\partial C_i}{\partial t} + \nabla \cdot (-D_i \nabla C_i) = \pm R_i \quad (6)$$

where  $C_i$  is the concentration of the species ( $\text{mol}/\text{m}^3$ ),  $D_i$  is the mass diffusion coefficient ( $\text{m}^2/\text{s}$ ) of species  $i$  in air. The values for  $D_i$  were obtained from the literature and are given in Table 2 [6, 16, 36]. In Eq. (6),  $R_i$  is the rate of generation of species  $i$  ( $\text{mol}/(\text{m}^3 \cdot \text{s})$ ) and was used

**Table 2** Mass diffusivity values of various reactive species in air

Species ( $i$ )	$D_{i,\text{air}}$ ( $\text{m}^2/\text{s}) \times 10^5$	Reference
$\text{O}_2$	1.9	[6]
$\text{O}_3$	3	[16]
$\text{O}$	6.1	[36]
$\text{OH}$	7.1	
$\text{H}_2\text{O}_2$	0.2	

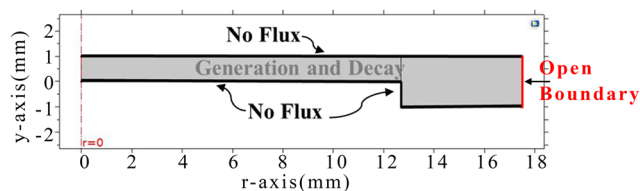


**Fig. 3** Boundary conditions for the transport of reactive species (no flux boundary condition at electrodes surfaces and glass surface and open boundary on the side) and generation and the decay between surfaces in the domain

to define decay or generation of reactive species  $\text{O}^{\bullet}$ ,  $\text{OH}$ ,  $\text{O}_3$ , and  $\text{H}_2\text{O}_2$  in the numerical simulation. The generation and the decay of the species were defined everywhere in the simulation domain (Fig. 3).

## Boundary conditions for predicting the distribution of charged species

The boundary conditions imposed in the mathematical model are described in Fig. 3. No flux boundary ( $J_i = 0$ ) condition was employed at electrode surfaces and the glass slide. The flux vector in the presence of the diffusion and reaction becomes,

$$J_i = -D_i \nabla C_i \quad (7)$$

Open boundary conditions were imposed on the side, which describes boundaries in contact with a large volume. The species can both enter and leave the domain from open boundaries, which can be described mathematically as follows.

$$\begin{cases} -n \cdot D_i \nabla C_i = 0 & \text{if } n \cdot u \geq 0 \\ C_i = C_{o,i} & \text{if } n \cdot u \leq 0 \end{cases} \quad (8)$$

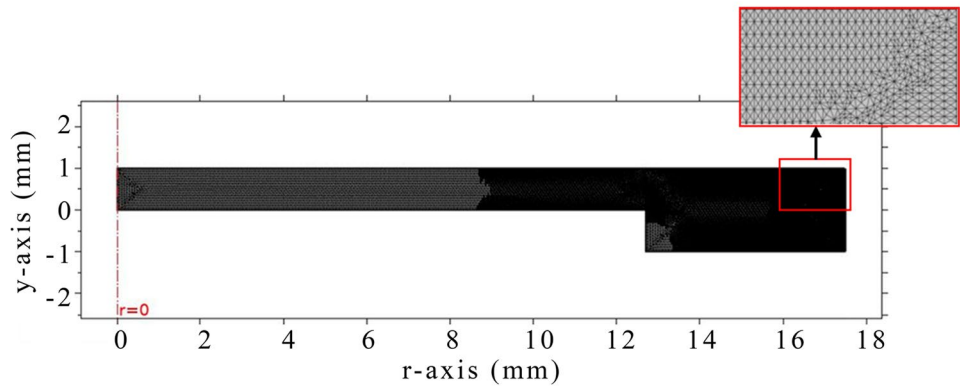
## Meshing for FE-DBD Plasma simulation

The computational domain was discretized using a triangular mesh. The mesh was generated by commercial software COMSOL Multiphysics® mesh generator module (Version 5.4). The initial mesh was finer and consisted of 10,119 triangles, 537 edge elements, and 7 vertex elements. During the numerical simulation runs, the computational mesh was adapted repeatedly based on the species concentration gradient until the mesh independent solution was obtained. The final grid had 19,187 triangles, 835 edge elements, and 7 vertex elements (Fig. 4).

## Solver and computational time

COMSOL Multiphysics® solver was used in the numerical simulation [8] and is based on an implicit time-dependent backward differentiation formula (BDF) solver algorithm. If the residual values for continuity and species concentration were all less than the user-defined relative tolerance value of  $10^{-3}$ , then the solution was considered to be converged. The computational time for a 2D axisymmetric model was 1 h and 47 min on a DELL Inc. workstation with Intel® Xeon® processor E5640 and 24 GB RAM.

**Fig. 4** Final computational mesh used for numerical simulation (19,187 triangles, 835 edge elements, and 7 vertex elements)



### Empirical microbial inactivation kinetics models

Microbial inactivation was assumed to follow a first-order reaction and therefore could be described as

$$S(t) = e^{-kt} \tag{9}$$

where  $S(t)$  is the survival ratio  $N/N_0$  at a given time, and  $t$  is the time (s).

The exponential model parameters  $k$  (1/s) was modified as a function of the numerically predicted reactive species concentration to predict the microbial inactivation kinetics of *E. aerogenes*.

$$k = \sum_1^i C_i k_i \tag{10}$$

where  $C_i$  (mol/m<sup>3</sup>) is the concentration of individual species, and  $k_i$  is the microbial inactivation rate of individual species (m<sup>3</sup>/(mol s)). The  $k_i$  values for reactive species were obtained from previous studies (Table 3) [1, 43, 49]. Microbial inactivation rate values for *Salmonella* were used in the calculations as *Salmonella* is closely related to *E. aerogenes*. The inactivation rate of H<sub>2</sub>O<sub>2</sub> was calculated based on the oxidation-reduction potential (ORP) of H<sub>2</sub>O<sub>2</sub> due to a lack of published inactivation data.

If we combine Eq. (9) and Eq. (10), we can rewrite the exponential model as a function of time and species concentration.

**Table 3** Microbial inactivation rate of *Salmonella* for individual reactive species

Species ( <i>i</i> )	$K_i$ (m <sup>3</sup> /(mol s))	Reference
H <sub>2</sub> O <sub>2</sub>	3.6	[49]
O <sub>3</sub>	3.9	[43]
OH	5.2	[1]

$$S(t) = \exp\left(-\left(\sum_1^i C_i k_i\right)t\right) \tag{11}$$

### Results and discussion

#### Identification of FE-DBD Plasma reactive species

Figures 5, 6, and 7 represent the typical emission spectrum from FE-DBD air plasma at three different frequencies (1 kHz, 2 kHz, and 3.5 kHz). The observed emission spectra illustrate the relative concentrations of nitrogen, oxygen, and hydrogen ions and their presence.

Atmospheric pressure cold air FE-DBD spectra showed emission peaks in all UV range (200–400 nm) and few in the visible light range. Metastable singlet state of oxygen (O I), oxygen (O II), nitrogen (N<sub>2</sub>R I), nitric oxide (NO I), hydroxyl radical (OHR I), and hydrogen ions (H<sub>2</sub> I) at

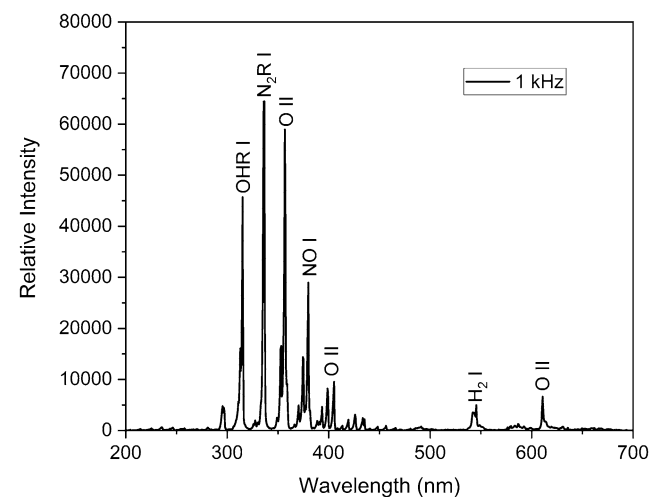


**Fig. 5** Emission spectra of FE-DBD plasma at 1 kHz in vis–NIR region (the gap between electrodes was 1 mm)

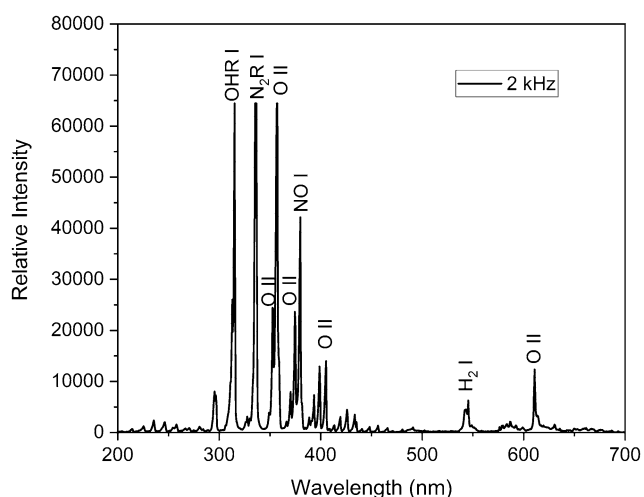


**Fig. 6** Emission spectra of FE-DBD plasma at 2 kHz in vis-NIR region (the gap between electrodes was 1 mm)

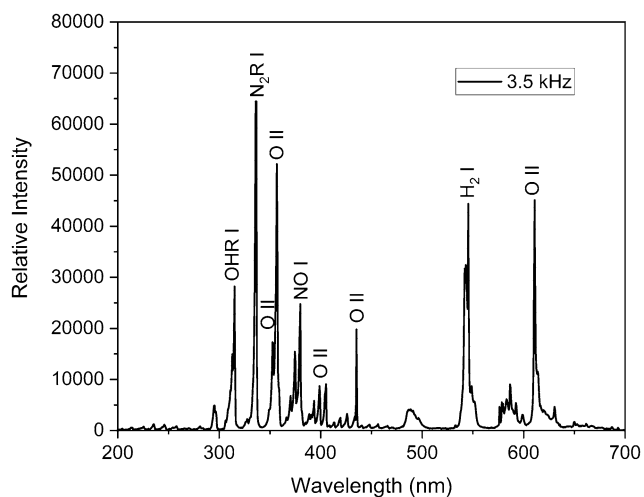


**Fig. 7** Emission spectra of FE-DBD plasma at 3.5 kHz in vis-NIR region (the gap between electrodes was 1 mm)

different energy states were detected, which would give way to the formation of antimicrobial reactive species via electron impact excitation and dissociation [46].

### Microbial inactivation efficacy of FE-DBD

Figure 8 represents the vegetative cell population (log CFU/surface) of *E. aerogenes* as a function of different FE-DBD plasma exposure times for three different frequencies. The average initial attached populations of *E. aerogenes* were  $7.12 \pm 0.05$ ,  $7.08 \pm 0.09$ , and  $7.11 \pm 0.09$  log CFU/surface at 1, 2, and 3.5 kHz, respectively. The

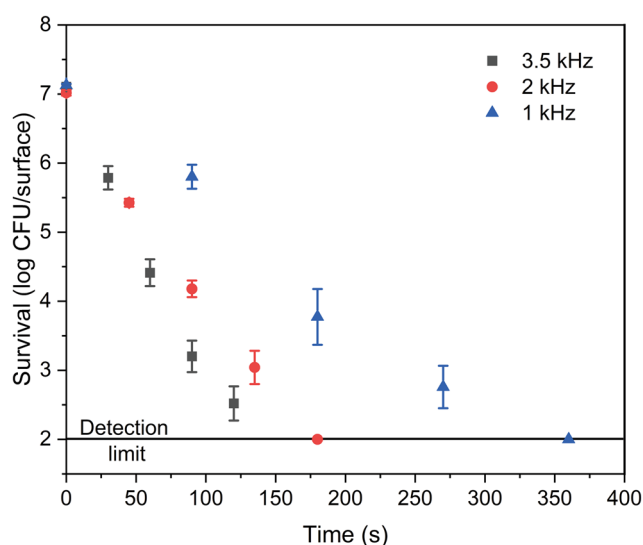


**Fig. 8** The effect of FE-DBD plasma treatment on microbial inactivation of *E. aerogenes* at three different frequencies (triangles, 1 kHz; circles, 2 kHz; squares, 3 kHz) at room temperature (the gap between electrodes was 1 mm, vertical bars indicate a standard error,  $n = 5$ )

results showed that the FE-DBD plasma was able to reduce the population of *E. aerogenes* by  $4.6 \pm 0.5$  log CFU/surface area at 3.5 kHz,  $5.1 \pm 0.09$  log CFU/surface area at 2 kHz, and  $5.1 \pm 0.05$  log CFU/surface area at 1 kHz on a glass surface in 120 s, 180 s, and 360 s, respectively ( $\pm$  indicates the standard error).

It is known that reactive species concentration increases with increasing frequency due to increased power input [52]. This results in a lower process time to achieve a similar level of inactivation at a higher frequency level (Fig. 8). The microbial inactivation efficacy (rate of inactivation) of FE-DBD decreased slightly with increasing process time. Such a slowing of the inactivation rate for multi-layered/stacked microorganisms has been reported by other researchers [22, 26, 51].

The FE-DBD plasma from the air contains reactive oxygen species, reactive nitrogen species, and UV radiation. It is possible that the achieved inactivation was due to the combined effect of all these components [44]. UV radiation might damage the cell membrane and promote production of peroxidases [27]. The reactive species can damage the cell membrane because of their high oxidation potential [18, 29]. Besides, the presence of nitrogen species inside the cell can alter the pH and the cell functionality [19].

Figure 9 evaluates the effect of the number of pulses on microbial inactivation efficacy of FE-DBD plasma, by plotting *E. aerogenes* concentration as a function of the number of pulses instead of time. There was no statistically significant difference observed in the rate of microbial inactivation per pulse at 3 different frequencies ( $p < 0.05$ ). It can be

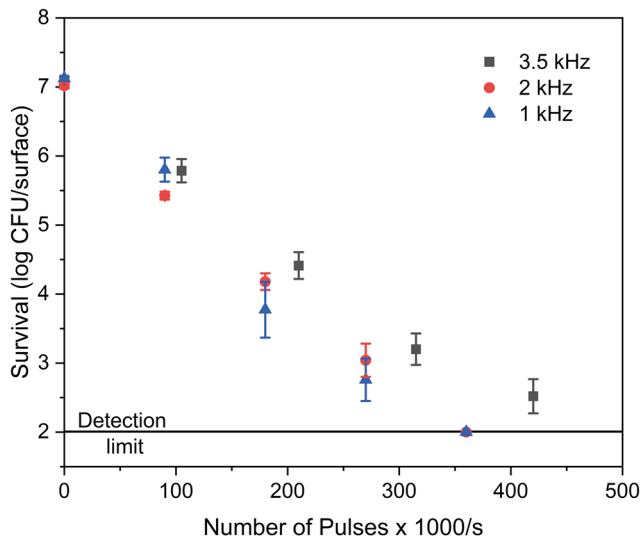


**Fig. 9** The effect of the number of pulses on microbial inactivation of *E. aerogenes* on a glass surface (triangles, 1 kHz; circles, 2 kHz; squares, 3 kHz) at room temperature (the gap between electrodes was 1 mm, vertical bars indicate a standard error,  $n = 5$ )

concluded that the rate of microbial inactivation per pulse was independent of frequency.

### Numerically predicted species distribution of FE-DBD Plasma system

Figures 10, 11, and 12 show the concentrations and the distributions of the predicted  $O^*$ , OH,  $O_3$ , and  $H_2O_2$  species at 1 kHz, 2 kHz, and 3.5 kHz, respectively. The amounts of reactive species increased with increased frequency. This increase can be explained by the increased power input. Higher frequency values increase the energy input, which results in a higher number of species generation in the FE-DBD plasma system.

Since diffusion was the only transport mechanism that was considered for calculating the species distributions in the FE-DBD plasma system, the concentrations of species were higher in the middle of the electrode, and the concentrations of species were lower along the edges of the electrodes.  $O_3$  and  $H_2O_2$  had higher predicted concentrations in the FE-DBD plasma system due to their greater stability and longer half-life which played an important role in microbial inactivation. The reactive oxygen species have been shown to have a larger contribution to lethality compared to other plasma components such as ions, UV light, or reactive nitrogen species [40, 41]. The numerical model assumed isothermal conditions and the effects of gravity (buoyancy) were not included. In an FE-DBD plasma, electrons are at a much higher temperature compared to the other particles such as ions and neutral species which are near room temperature.

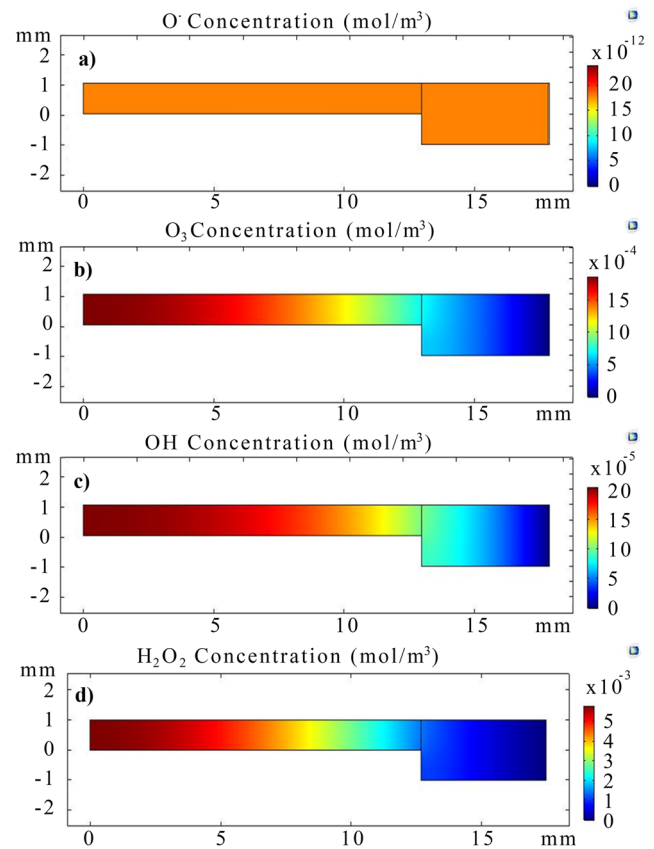


**Fig. 10** Concentration distribution of **a**  $O^*$ , **b**  $O_3$ , **c** OH, and **d**  $H_2O_2$  in the FE-DBD plasma after steady state at 1 kHz

Since FE-DBD plasma is dominated by ions and neutral particles, the effect of temperature on the movement of plasma species due to buoyancy can be considered negligible [9].

### Comparison between numerical predictions and experimental data for microbial inactivation in an FE-DBD plasma system

Comparisons between numerical predictions using a modified exponential model (Eq. 10 and Eq. 11) with an average concentration of numerically predicted OH,  $H_2O_2$ , and  $O_3$  species at the interacting surface and experimental results at the three frequencies are shown in Figs. 13, 14, and 15.

Microbial inactivation model based on reactive species predicted 4.1, 4.6, and 4.5 log CFU/surface reduction in the population of *E. aerogenes* for 360, 180, and 120 s of FE-DBD plasma processing, at 1 kHz, 2 kHz, and 3.5 kHz, respectively. A maximum difference of 1 log was observed between the numerical predictions and the experimental results. There are several possible explanations for this difference. The numerical simulation domain was taken to be two-dimensional axisymmetric without swirl to save on computational time. For the simulation purposes, the square



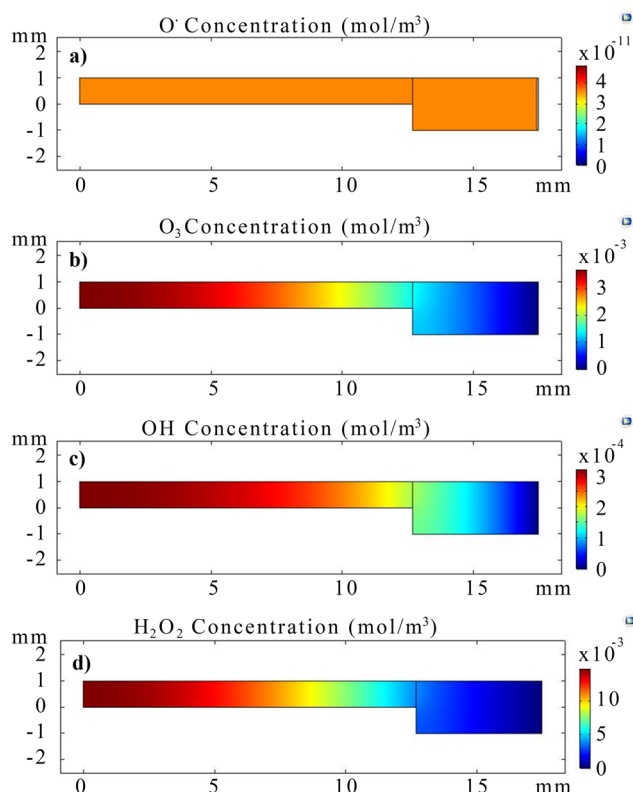


**Fig. 11** Concentration distribution of **a** O<sup>•</sup>, **b** O<sub>3</sub>, **c** OH, and **d** H<sub>2</sub>O<sub>2</sub> in the FE-DBD plasma after steady state at 2 kHz

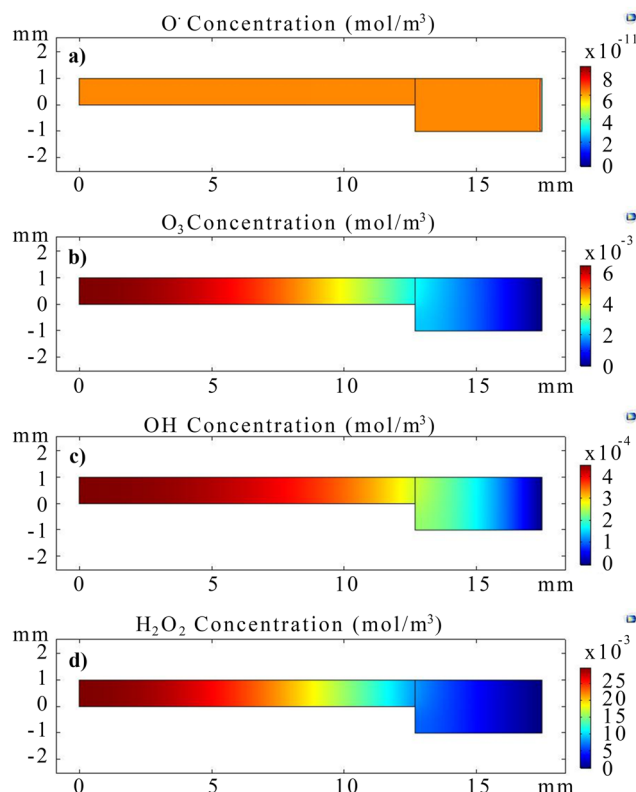


**Fig. 12** Concentration distribution of **a** O<sup>•</sup>, **b** O<sub>3</sub>, **c** OH, and **d** H<sub>2</sub>O<sub>2</sub> in the FE-DBD plasma after steady state at 3.5 kHz

inoculated region on the glass slide was approximated by a circumscribed circle. The numerical simulation also did not include microbial inactivation due to singlet oxygen, superoxide, nitric oxide, and UV and their combined effect [22, 44]. Only reactive oxygen species were included in the predictive model. This could explain the underprediction of microbial inactivation by numerical simulation model compared to experimental data.

It has been reported that plasma operating pressure influences the generation of UV radiation. Low pressure plasma, i.e., vacuum plasma could potentially release UV at the range between 200 and 290 nm [38]. Atmospheric pressure plasma generally emits UV radiation between 305 and 390 nm. UV radiation in this range is not effective enough to inactivate microorganisms [47]. Many researchers have reported that UV radiation has minimal or no significant effect in terms of microbial inactivation in atmospheric plasma processing. There is no general agreement among researchers on the role of UV radiation in atmospheric pressure plasma decontamination processes [14, 15, 17, 29, 37]. Hasan [15] used a log-linear model based on reactive species to predict microbial inactivation and included a UV component in the model. But the effect of UV in that predictive model was found to be minimal compared to the effect of

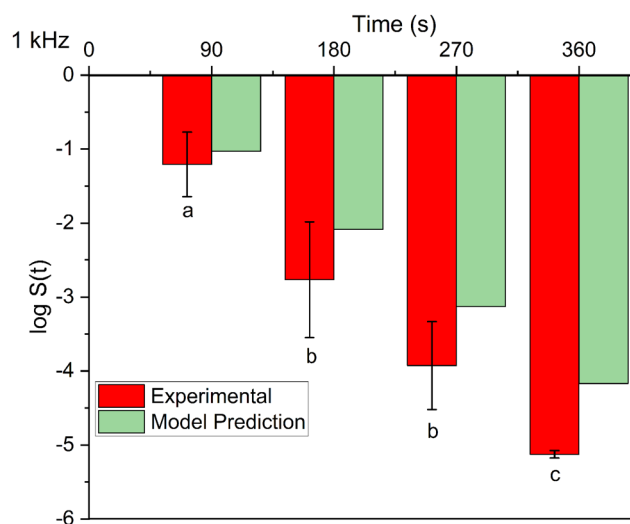


**Fig. 13** Experimental and predicted microbial inactivation kinetics of *E. aerogenes* at 1 kHz for FE-DBD plasma system (error bars indicate the standard deviations and  $n = 5$ ; data that do not share the same letter are significantly different ( $P < 0.05$ ))

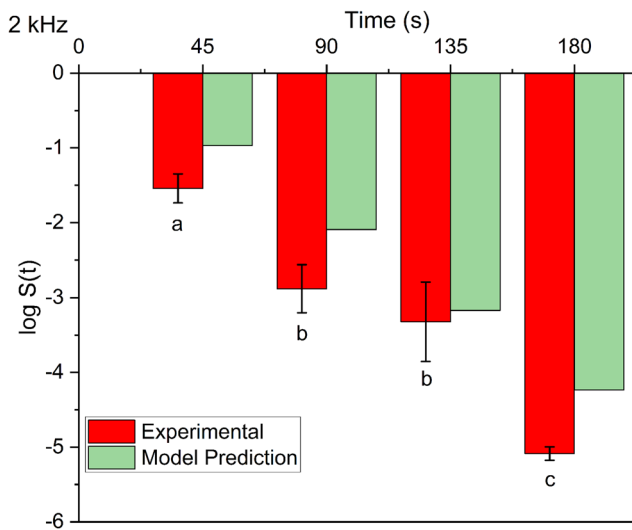


**Fig. 14** Experimental and predicted microbial inactivation kinetics of *E. aerogenes* at 2 kHz for FE-DBD plasma system (error bars indicate standard deviations and  $n = 5$ ; data that do not share the same letter are significantly different ( $P < 0.05$ ))

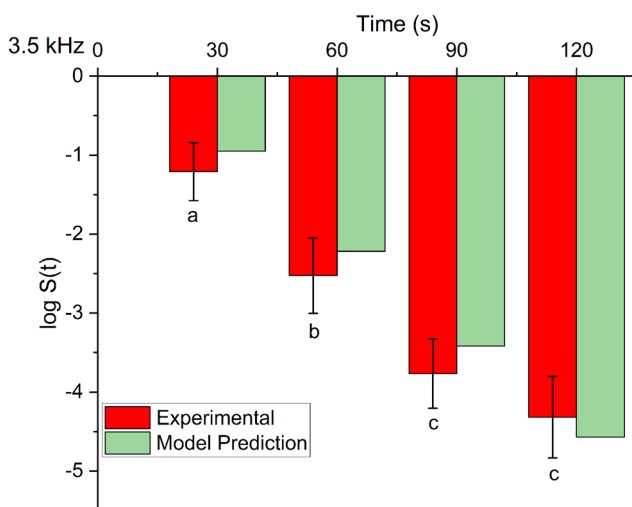


**Fig. 15** Experimental and predicted microbial inactivation kinetics of *E. aerogenes* at 3.5 kHz for FE-DBD plasma system (error bars indicate the standard deviations and  $n = 5$ ; data that do not share the same letter are significantly different ( $P < 0.05$ ))

reactive species in the plasma. The model can be improved by including more species (e.g., reactive nitrogen species, peroxy nitrate, etc.), which would also require testing the microbial inactivation efficacy of each reactive species individually. This would also potentially require the addition of models for the interaction effects of UV and reactive species.

The model also over predicted microbial inactivation at 3.5 kHz for 2 min. This might be explained by the detection limit of the total plate count method. There were no colonies recovered at 3.5 kHz for 2 min plasma process conditions,

and the plate count detection limit was 2 log CFU/surface. There might be more than 5 log inactivation on those conditions after plasma processing, but it could not be confirmed due to the inherent limits of the plate count method. To make use of any novel process (including plasma technology) in the food industry, the process must be understood or at least be predictable to a large degree. The results of this study give a preliminary understanding of complexities inherent in the prediction of microbial inactivation by plasma. These results should help in the design of plasma equipment or may provide a starting point for future microbial inactivation experiments.

In order to find out the effect of the variation in the G-value on the numerically predicted microbial inactivation, the numerical simulation was carried out by using G-values with  $\pm 10\%$  error. Microbial inactivation increased by about 12% at 10% higher G-value and decreased by about 12% at 10% lower G-value, which was not unexpected.

## Conclusions

We experimentally investigated microbial inactivation efficacy of FE-DBD and developed an empirical microbial inactivation model as a function of numerically predicted reactive species. The inactivation model used a COMSOL® Multiphysics-based numerical simulation model to predict reactive species concentrations and distributions in the FE-DBD system. The predicted species concentrations were used to estimate microbial inactivation kinetics. Our results showed that FE-DBD plasma treatment reduced the population of *E. aerogenes* on the model system by up to 5 log CFU/surface. The microbial inactivation model based on numerically predicted reactive species and microbial inactivation rate from the literature were under-predicted microbial inactivation compared to experimental results. There was a maximum of 1 log difference between the prediction results and the experimental results.

**Acknowledgement** Authors would like to thank C. & J. Nyheim Plasma Institute, Drexel University Plasma Agricultural laboratory members for their help in the operation of FE-DBD plasma; Dr. Juzhong Tan, Department of Food Science, Rutgers University, for his valuable inputs.

**Funding** This study is financially supported by the Turkish Ministry of Education. Partial funding is provided by the New Jersey Agricultural Experiment Station.

## References

1. Back KH, Ha JW, Kang DH (2014) Effect of hydrogen peroxide vapor treatment for inactivating *Salmonella typhimurium*, *Escherichia coli* O157: H7 and *Listeria monocytogenes* on organic fresh

- lettuce. *Food Control* 44:78–85. <https://doi.org/10.1016/j.foodcont.2014.03.046>
2. Berlett BS, Stadtman ER (1997) Protein oxidation in aging, disease, and oxidative stress. *J Biol Chem* 272(33): 20313–20316. <https://doi.org/10.1074/jbc.272.33.20313>
  3. Bhide S, Salvi D, Schaffner DW, Karwe MV (2017) Effect of surface roughness in model and fresh fruit systems on microbial inactivation efficacy of cold atmospheric pressure plasma. *J Food Prot* 80(8): 1337–1346. <https://doi.org/10.4315/0362-028X.JFP-17-064>
  4. Bourke P, Ziuzina D, Han L, Cullen PJ, Gilmore BF (2017) Microbiological interactions with cold plasma. *J Appl Microbiol* 123(2): 308–324. <https://doi.org/10.1111/jam.13429>
  5. Boxhammer V, Morfill GE, Jokipii JR, Shimizu T, Klämpfl T, Li Y-F, Köritzer J, Schlegel J, Zimmermann JL (2012) Bactericidal action of cold atmospheric plasma in solution. *New J Phys* 14(11): 113042. <https://doi.org/10.1088/1367-2630/14/11/113042>
  6. Cussler EL (1985) Diffusion: mass transfer in fluid systems. *AIChE J* 31(3): 523–523. <https://doi.org/10.1002/aic.690310333>
  7. d'Agostino R, Favia P, Oehr C, Wertheimer MR (2005) Low-temperature plasma processing of materials: past, present, and future. *Plasma Processes. Polym* 2(1): 7–15. <https://doi.org/10.1002/ppap.200400074>
  8. Dickinson EJ, Ekström H, Fontes E (2014) “COMSOL Multiphysics®: finite element software for electrochemical analysis. A mini-review.” *Electrochemistry Communications* 40: 71–74. <https://doi.org/10.1016/j.elecom.2013.12.020>
  9. Fridman A (2008) *Plasma chemistry*. Cambridge University Press Cambridge. <https://doi.org/10.1017/CBO9780511546075>
  10. Fridman G, Peddinghaus M, Ayan H, Fridman A, Balasubramanian M, Gutsol A, Brooks A, Friedman G (2006) Blood coagulation and living tissue sterilization by floating-electrode dielectric barrier discharge in air. *Plasma Chem Plasma Process* 26(4): 425–442. <https://doi.org/10.1007/s11090-006-9024-4>
  11. Gaunt LF, Beggs CB, Georghiou GE (2006) Bactericidal action of the reactive species produced by gas-discharge nonthermal plasma at atmospheric pressure: a review. *IEEE Transactions on Plasma Science* 34(4II): 1257–1269. <https://doi.org/10.1109/TPS.2006.878381>
  12. Grzegorzewski F, Rohn S, Quade A, Schröder K, Ehlbeck J, Schlüter O, Kroh LW (2010) Reaction chemistry of 1,4-benzopyrone derivatives in non-equilibrium low-temperature plasmas. *Plasma Processes Polym* 7(6): 466–473. <https://doi.org/10.1002/ppap.200900140>
  13. Grzegorzewski F, Schlüter O, Ehlbeck J, Weltmann KD, Geyer M, Kroh LW, Rohn S (2009) Plasma-oxidative degradation of polyphenolics - influence of non-thermal gas discharges with respect to fresh produce processing. *Czech Journal of Food Sciences* 27 (SPEC. ISS.): 35–39. <https://doi.org/10.17221/1107-cjfs>
  14. Hajhoseini A, Sharifan A, Yousefi HR (2020) Effects of atmospheric cold plasma on microbial growth of *Listeria innocua* and *Staphylococcus aureus* in ready-to-eat fish products. *Iranian Journal of Fisheries Sciences* 19(1): 262–271. <https://doi.org/10.22092/ijfs.2019.119545>
  15. Hasan MHA (2011) Phenomenological estimation of plasma sterilization kinetics. Drexel University. <https://hdl.handle.net/1860/3724>
  16. Hegeler F, Akiyama H (1997) Spatial and temporal distributions of ozone after a wire-to-plate streamer discharge. *Digest of Technical Papers-IEEE International Pulsed Power Conference* 2(5): 1085–1090. <https://doi.org/10.1109/ppc.1997.674541>
  17. Herrmann HW, Henins I, Park J, and Selwyn GS (1999) Decontamination of chemical and biological warfare (CBW) agents using an atmospheric pressure plasma jet (APPJ). *Physics of Plasmas* 6(5 I): 2284–89. <https://doi.org/10.1063/1.873480>
  18. Hertwig C, Leslie A, Meneses N, Reineke K, Rauh C, Schlüter O (2017) Inactivation of *Salmonella enteritidis* PT30 on the surface of unpeeled almonds by cold plasma. *Innovative Food Science and Emerging Tech* 44:242–248. <https://doi.org/10.1016/j.ifset.2017.02.007>
  19. Hertwig C, Reineke K, Ehlbeck J, Erdoidu B, Rauh C, Schlüter O (2015) Impact of remote plasma treatment on natural microbial load and quality parameters of selected herbs and spices. *J Food Eng* 167:12–17. <https://doi.org/10.1016/j.jfoodeng.2014.12.017>
  20. Jiang J, Lu Y, Li J, Li L, He X, Shao H, Dong Y (2014) Effect of seed treatment by cold plasma on the resistance of tomato to *Ralstonia solanacearum* (bacterial wilt). *Plos One* 9(5): 1–6. <https://doi.org/10.1371/journal.pone.0097753>
  21. Joshi I, Salvi D, Schaffner DW, Karwe MV, (2018) Characterization of microbial inactivation using plasma-activated water and plasma-activated acidified buffer. *J Food Prot* 81(9): 1472–1480. <https://doi.org/10.4315/0362-028X.JFP-17-487>
  22. Joshi SG, Cooper M, Yost A, Paff M, Ercan UK, Fridman G, Friedman G, Fridman A, Brooks AD, (2011) Nonthermal dielectric-barrier discharge plasma-induced inactivation involves oxidative DNA damage and membrane lipid peroxidation in *Escherichia coli*. *Anti Agents Chemo* 55(3): 1053–1062. <https://doi.org/10.1128/AAC.01002-10>
  23. Kim HS, Cho YI, Hwang IH, Lee DH, Cho DJ, Rabinovich A, Fridman A (2013) Use of plasma gliding arc discharges on the inactivation of *E. coli* in water. *Sep Purif Technol* 120: 423–428. <https://doi.org/10.1016/j.seppur.2013.09.041>
  24. Kim HH (2004) Nonthermal plasma processing for air-pollution control: a historical review, current issues, and future prospects. *Plas Proc Polym* 1(2): 91–110. <https://doi.org/10.1002/ppap.200400028>
  25. Kim HJ, Yong HI, Park S, Choe W, Jo C (2013) Effects of dielectric barrier discharge plasma on pathogen inactivation and the physicochemical and sensory characteristics of pork loin. *Curr Appl Phys* 13(7): 1420–1425. <https://doi.org/10.1016/j.cap.2013.04.021>
  26. Kostov KG, Rocha V, Koga-Ito CY, Matos BM, Algatti MA, Honda RY, Kayama ME, Mota RP (2010) Bacterial sterilization by a dielectric barrier discharge (DBD) in air. *Surf Coat Technol* 204(18–19): 2954–2959. <https://doi.org/10.1016/j.surfcoat.2010.01.052>
  27. Koutchma, Tatiana. 2019. Ultraviolet light in food technology: principles and applications. <https://doi.org/10.1201/9780429244414>.
  28. Krieg RE, Lockhart WR (1966) Classification of enterobacteria based on overall similarity. *J Bacteriol* 92(5): 1275–1280. <https://doi.org/10.1128/jb.92.5.1275-1280.1966>
  29. Laroussi M (1996) “Sterilization of contaminated matter with an atmospheric pressure plasma” 24(3): 1188–1191. <https://doi.org/10.1109/27.533129>.
  30. Lee K, Paek K-h, Ju W-T, Lee Y et al (2006) Sterilization of bacteria, yeast, and bacterial endospores by atmospheric-pressure cold plasma using helium and oxygen. *J. Microbio* (Seoul, Korea) 44(3): 269–275. <https://www.ncbi.nlm.nih.gov/pubmed/16820756>
  31. Liu B, Schaffner DW (2007) Quantitative analysis of the growth of *Salmonella stanley* during alfalfa sprouting and evaluation of *Enterobacter aerogenes* as its surrogate. *J Food Prot* 70(2): 316–322. <https://doi.org/10.4315/0362-028X-70.2.316>
  32. Loeb LB (1956) Basic processes of gaseous electronics. *Phys Today* 9(5) 29–30. <https://doi.org/10.1063/1.3059964>
  33. Maisch T, Shimizu T, Li YF, Heinlin J, Karrer S, Morfill G, Zimmermann JL (2012) Decolonisation of MRSA, *S. aureus* and *E. coli* by cold-atmospheric plasma using a porcine skin model in vitro. *PLoS ONE* 7(4): 1–9. <https://doi.org/10.1371/journal.pone.0034610>

34. Mancini RA, Hunt MC (2005) Current research in meat color. *Meat Sci* 71(1): 100–121. <https://doi.org/10.1016/j.meatsci.2005.03.003>
35. Manion JA, Huie RE, Levin RD, Burgess DR, Jr, Orkin VL, Tsang W, McGivern WS, et al. (2015) “NIST Standard Reference Database 17, Version 7.0 (Web Version).” National Institute of Standards and Technology. 2015. <https://kinetics.nist.gov/kinetics/citation.jsp>
36. Martinez I (2019) “Mass Diffusivity Data.” 2019. [https://webserver.dmt.upm.es/~isidoro/dat1/Mass\\_diffusivitydata.pdf](https://webserver.dmt.upm.es/~isidoro/dat1/Mass_diffusivitydata.pdf).
37. Moldgy A, Hamada A, Gaurav N, Sagar and Bruggeman P (2020) “Comparative evaluation of the virucidal effect of remote and direct cold air plasmas with UV-C.” *Plasma Processes and Polymers* 17(4). <https://doi.org/10.1002/ppap.201900234>.
38. Munakata N, Hidea K, Kobayashi K, Ito A, Ito T (1986) Action spectra in ultraviolet wavelengths (150–250 Nm) for inactivation and mutagenesis of *Bacillus subtilis* spores obtained with synchrotron radiation. *Photochem Photobiol* 44(3): 385–390. <https://doi.org/10.1111/j.1751-1097.1986.tb04680.x>
39. Oehmigen K, Winter J, Hähnel M, Wilke C, Brandenburg R, Weltmann KD, Von Woedtke T (2011) Estimation of possible mechanisms of *Escherichia coli* inactivation by plasma treated sodium chloride solution *Plasma Processes Polym* 8(10): 904–913. <https://doi.org/10.1002/ppap.201000099>
40. Pai K, Timmons C, Roehm KD, Ngo A, Narayanan SS, Ramachandran A, Jacob JD, Ma LM, Madihally SV (2018) Investigation of the roles of plasma species generated by surface dielectric barrier discharge *Scientific Reports* 8(1): 1–13. <https://doi.org/10.1038/s41598-018-35166-0>
41. Perni S, Liu DW, Shama G, Kong MG (2008) Cold atmospheric plasma decontamination of the pericarps of fruit. *J Food Prot* 71(2): 302–308. <https://doi.org/10.4315/0362-028X-71.2.302>
42. Perni S, Shama G, Hobman JL, Lund PA, Kershaw CJ, Hidalgo-Arroyo GA, Penn CW, Deng XT, Walsh JL, Kong MG (2007) Probing bactericidal mechanisms induced by cold atmospheric plasmas with *Escherichia coli* mutants. *Appl Phys Lett* 90(7): 10–13. <https://doi.org/10.1063/1.2458162>
43. Rodriguez-Romo LA, Yousef AE (2005) Inactivation of *Salmonella enterica* serovar enteritidis on shell eggs by ozone and UV radiation. *J Food Prot* 68(4): 711–717. <https://doi.org/10.4315/0362-028X-68.4.711>
44. Sarangapani C, Patange A, Bourke P, Keener K, Cullen PJ (2018) Recent advances in the application of cold plasma technology in foods. *Annual Review of Food Science and Technology* 9(1): 609–629. <https://doi.org/10.1146/annurev-food-030117-012517>
45. Shi XM, Zhang GJ, Wu XL, Li YX, Ma Y, Shao XJ (2011) Effect of low-temperature plasma on microorganism inactivation and quality of freshly squeezed orange juice. *IEEE Trans Plasma Sci* 39(7): 1591–1597. <https://doi.org/10.1109/TPS.2011.2142012>
46. Smirnov SA, Rybkin VV, Kholodkov IV, Titov VA (2002) Simulation of the processes of formation and dissociation of neutral particles in air plasma: kinetics of neutral components. *High Temp* 40(3): 323–330. <https://doi.org/10.1023/A:1016030520696>
47. Stoffels E, Sakiyama Y, Graves DB et al (2008) Cold atmospheric plasma: charged species and their interactions with cells and tissues. *IEEE Transactions on Plasma Science* 36 (4 PART 2): 1441–1457. <https://doi.org/10.1109/TPS.2008.2001084>
48. Surowsky B, Fröhling A, Gottschalk N, Schlüter O, Knorr D (2014) Impact of cold plasma on *Citrobacter freundii* in apple juice: inactivation kinetics and mechanisms. *Int J Food Microbiol* 174: 63–71. <https://doi.org/10.1016/j.ijfoodmicro.2013.12.031>
49. Surowsky B, Schlüter O, Knorr D (2015) Interactions of non-thermal atmospheric pressure plasma with solid and liquid food systems: a review. *Food Engineering Reviews* 7(2): 82–108. <https://doi.org/10.1007/s12393-014-9088-5>
50. Trivedi MH, Patel K, Itokazu H, Huynh NA, Kovalenko M, Nirenberg G, Miller V (2019) Enhancing shelf life of bananas by using atmospheric pressure pulsed cold plasma treatment of the storage atmosphere. *Plasma Medicine* 9(1): 23–38. <https://doi.org/10.1615/PlasmaMed.2019026909>
51. Woedtke T, von Kramer A, Weltmann KD (2008) Plasma sterilization: what are the conditions to meet this claim? *Plasma Processes Polym* 5(6): 534–539. <https://doi.org/10.1002/ppap.200800013>
52. Zhang H, Xu Z, Shen J, Li X, Ding L, Ma J, Lan Y et al (2015) Effects and mechanism of atmospheric-pressure dielectric barrier discharge cold plasma on lactate dehydrogenase (LDH) enzyme. *Scientific Reports* 5(March): 1–12. <https://doi.org/10.1038/srep10031>
53. Zhao P, Zhao T, Doyle , Rubino JR, Meng J (1998) Development of a model for evaluation of microbial cross-contamination in the kitchen. *J Food Prot* 61(8): 960–963. <https://doi.org/10.4315/0362-028X-61.8.960>

**Publisher's Note** Springer Nature remains neutral with regard to jurisdictional claims in published maps and institutional affiliations.